Platform for Electrically Pumped Polariton Simulators and Topological Lasers

Holger Suchomel, Sebastian Klembt, Tristan H. Harder, Martin Klaas, Oleg A. Egorov, Karol Winkler, Monika Emmerling, Ronny Thomale, Sven Höfling, and Christian Schneider

Phys. Rev. Lett. **121**, 257402 — Published 21 December 2018

DOI: 10.1103/PhysRevLett.121.257402

A platform for electrically pumped polariton simulators and topological lasers

Holger Suchomel,[1,*] Sebastian Klembt,[1,†] Tristan H. Harder,[1] Martin Klaas,[1] Oleg A. Egorov,[1] Karol Winkler,[1] Monika Emmerling,[1] Ronny Thomale,[2] Sven Höfling,[1,3] and Christian Schneider[1]

[1] *Technische Physik, Wilhelm-Conrad-Röntgen-Research Center for Complex Material Systems, Universität Würzburg, Am Hubland, D-97074 Würzburg, Germany*

[2] *Institut für Theoretische Physik, Universität Würzburg, Am Hubland, D-97074 Würzburg, Germany*

[3] *SUPA, School of Physics and Astronomy, University of St Andrews, St Andrews KY16 9SS, United Kingdom*

Two-dimensional electronic materials such as graphene and transition metal dichalgenides feature unique electrical and optical properties due to the conspirative effect of band structure, orbital coupling, and crystal symmetry. Synthetic matter, as accomplished by artificial lattice arrangements of cold atoms, molecules, electron patterning, and optical cavities, has emerged to provide manifold intriguing frameworks to likewise realize such scenarios. Exciton-polaritons have recently been added to the list of promising candidates for the emulation of system Hamiltonians on a semiconductor platform, offering versatile tools to engineer the potential landscape and to access the non-linear electro-optical regime. In this work, we introduce an electronically driven square and honeycomb lattice of exciton-polaritons, paving the way towards real world devices based on polariton lattices for on-chip applications. Our platform exhibits laser-like emission from high-symmetry points under direct current injection, hinting at the prospect of electrically driven polariton lasers with possibly topologically non-trivial properties.

I. INTRODUCTION

Microcavity exciton-polaritons (polaritons) are composite bosonic particles originating from the strong coupling between excitons and microcavity photons [1]. Their bosonic nature, strong nonlinearities, as well as their convenient accessibility by angular-resolved photo- or electroluminescence (PL and EL) spectroscopy put them in the focus of contemporary fundamental research devoted to macroscopic quantum phases in solid state systems, culminating in the observation of collective bosonic behaviour manifest in Bose-Einstein condensation [2–4] and superfluidity [5]. Furthermore, even the classical operational limit of polariton lattices has triggered significant interest due to the prospect of enabling detailed model engineering towards artificial topological matter [6–8], which has recently peaked in the experimental implementation of optically driven topological polariton lasers [9] and polariton Chern insulators [10].

Previously studied in a variety of material systems [11–14] and microcavity architectures [15–18], the currently highest quality devices for polaritons are based on epitaxially grown III-V distributed Bragg reflectors (DBRs) with embedded GaAs quantum wells (QWs) [19], where techniques derived from semiconductor nanotechnology could be fruitfully employed [20–25]. In order to accomplish a tunable lattice arrangement of microcavities, micropillar etching is employed to implement deep potentials along with a careful tuning of the pillar proximity and overlap in order to enable lattice hybridization (hopping) [26, 27]. It has led to the design of polariton band structures on the square [28, 29], Lieb [30, 31], Kagome [32], and honeycomb lattice [25, 33]. Along with other degrees of freedom constituting candidates for synthetic matter such as microwave cavities, photonic crystals, waveguides, and electric circuits, polariton lattices are evolving into a promising platform for emulating topological states of matter [6–8]. As a distinguishing advantage towards opto-electronic applications, however, polaritons allow not only optical but also electrical driving, which is likely indispensable for any vision of on-chip technology, and likewise, real world applications. Techniques for direct current injection into polariton states [35], including the nonlinear regime of bosonic condensation [36, 37] have been developed, and represent an important tool for practical plug-and-play implementations [38, 39].

In this work, we present a technology platform facilitating electrical injection into arbitrary two-dimensional lattice geometries hosting polaritons, and study the band structure formation in an electrically pumped square- and honeycomb lattice in the strong coupling limit, both in the linear and non-linear regime. We demonstrate that we can electrically drive ~ 250 lattice sites in the tight-binding (TB) limit, marking a step change in engineering of photonic lattices in general. We observe polariton band structures that exhibit good agreement with the TB description of the lowest energy band (S-band) for a square and honeycomb lattice, the latter exhibiting its distinct K and K' points, and the corresponding Dirac cone dispersion reminiscent of graphene [34].

* holger.suchomel@physik.uni-wuerzburg.de

† sebastian.klembt@physik.uni-wuerzburg.de

H. Suchomel and S. Klembt contributed equally to this work.

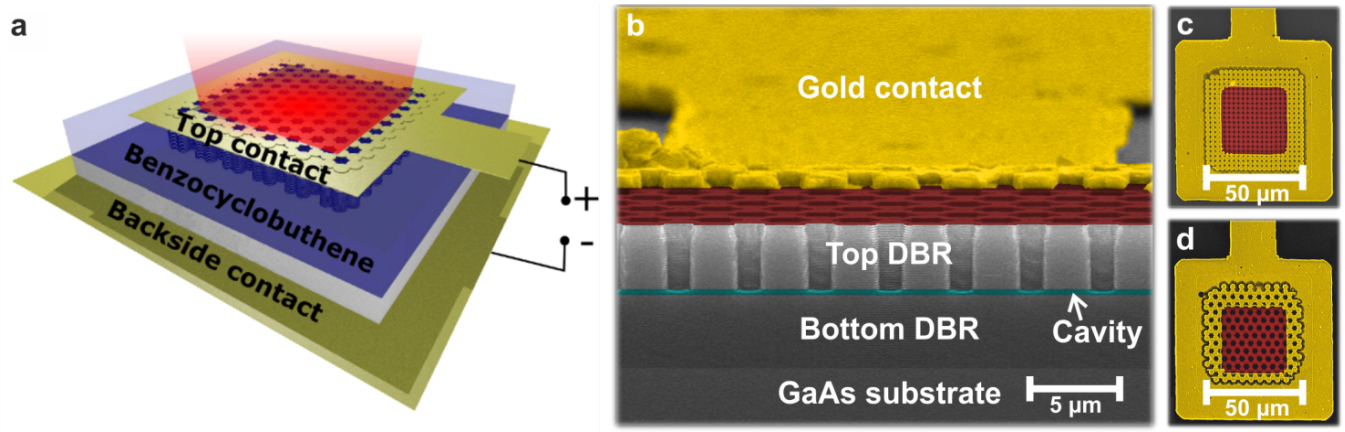

FIG. 1. (a) Schematic of the investigated device showing the half-etched polariton lattice, planarized with benzocyclobutene with top and bottom electrical contacts. (b) Scanning electron microscope (SEM) image of the processed device with a view tilted above the cleaved edge, cutting the device in half. A gold contact (yellow) has been deposited on an etched two-dimensional lattice (red) in order to inject a current into the microcavity structure. The quantum wells (QWs) have been placed in the field maximum inside a λ-cavity (cyan). The n-contact is deposited on the plane backside of the GaAs substrate. To avoid etching damage to the QWs, the etching depth has been adjusted in order to stop close above the cavity region. (c-d) SEM images of the investigated lattice devices in top view configuration. The deposited gold contact (yellow) surrounds the etched lattices (red) with an overlap of one to two lattice constants. The whole lattice field has an edge length of ~ 50 μm with (c) depicting the investigated square lattice and (d) the honeycomb lattice.

II. EXPERIMENTAL SETUP

A. Implementation

The polariton device is based on a pin-doped, vertically emitting microcavity structure with 27 $Al_{0.20}Ga_{0.80}As$/AlAs mirror pairs in the p-doped top distributed Bragg reflector (DBR), 31 $Al_{0.20}Ga_{0.80}As$/AlAs mirror pairs in the n-doped bottom DBR, and a single stack of four GaAs QWs embedded in the field antinode of the intrinsic $Al_{0.40}Ga_{0.60}As$ λ-wavelength-thick cavity. The cavity structure was grown by molecular beam epitaxy on a n-doped GaAs substrate. We characterized the wafer via white-light reflectance measurements at 10 K by using the spatial variation of the cavity resonance and extracted a Rabi splitting of $\hbar\Omega_R = (5.4 \pm 0.1)$ meV in the presence of the built-in potential from the unbiased pin-junction. The quality factor of the cavity was extracted from PL measurements on a far-red-detuned area of the wafer, yielding a value of Q $\sim$ 15,000. A detailed description of the sample growth, doping profile and basic optical properties can be found in the Supplementary Material.

The electrically injected polaritonic lattices, schematically depicted in Fig. 1a, were implemented on the microcavity structure by a series of processing steps. First, an AuGe-Ni-Au alloy was evaporated and annealed on the backside of the substrate serving as the n-contact. In order to generate the 2D polariton lattices, square as well as honeycomb lattices were defined by electron beam lithography. After the deposition of BaF_2 as an etching mask and the subsequent lift-off step, the structures were etched using electron cyclotron resonance-reactive ion etching. Here, the etching depth is calibrated such that only the top DBR is etched and the cavity with the embedded QWs remains intact (see scanning electron microscope (SEM) image Fig. 1b, Supplementary Material, Fig. S1c). Current injection is provided by fabricating electrically contacted frames overlapping with one to two lattice constants of the lattice. In order to generate a platform for the contacting step at the p-doped side of the structure, the sample was planarized with the transparent polymer benzocyclobutene (BCB) using a thin layer of sputtered Si_3N_4 as an adhesive layer (Supplementary Material, Fig. S1d). Besides serving as a platform for the contact level, the BCB is also used as an electrical insulation between different devices and to prevent oxidation of the exposed lattice sidewalls. Finally, the contact level on top of the planarized sample was defined via optical lithography and evaporation of an Au-Cr alloy. The following lift-off step completes the device processing. Side, as well as top view images of the contacted square and honeycomb lattices are shown in Figs. 1b-d. The width of a full lattice array amounts to 50 μm.

B. Experiment

We characterize our processed devices by momentum resolved PL and EL spectroscopy. For the PL measurements, we excite our sample by a 2 ps pulsed Ti:sapphire laser with a repetition rate of 82 MHz. For each device the laser energy was tuned to the reflectance minimum of the first high-energy Bragg mode around $\sim$ 84 meV above the emission energy. In the case of the EL measurements, the sample was excited by applying a DC bias between

the backside and top contact using a standard voltage source. The injected current was determined by measuring the voltage drop across a series resistance of 1 kΩ. In both excitation configurations, the luminescence is collected using a Fourier spectroscopy setup with a Czerny-Turner monochromator and a Peltier-cooled 1024x1024 px CCD operating at -100 °C. By motorized scanning of the last imaging lens we can collect the full dispersion information in the k_x- and k_y-directions. All following experiments on the processed devices have been carried out at a sample temperature of $\sim$ 4 K.

III. RESULTS AND DISCUSSION

A. Honeycomb Lattice

A lattice geometry which attracted a substantial interest in emulating two-dimensional Hamiltonians is the graphene lattice, made up of single sites arranged in a honeycomb configuration. The SEM image in Fig. 2a depicts the honeycomb lattice studied in this article with the two-element base as well as the primitive lattice vectors being highlighted. The corresponding reciprocal lattice is shown in Fig. 2b. The 1st Brillouin zone (BZ) includes the high symmetry points M, K, and K′ at the edge and Γ in the center. The ratio between the pillar diameters of $d = 3.0$ μm to the lattice constant of $a = 2.7$ μm amounts to ~ 0.9. We characterize the optical properties of the lattice by non-resonant laser excitation. The photon-exciton detuning was estimated by treating the lowest energy of the measured band structure as the polariton branch which arises due to the coupling between the heavy hole QW exciton (Supplementary Material, Fig. S2) and the photon mode spectrum of a single 3.0 μm micropillar [36]. In doing so, the photon-exciton detuning amounts to -2.3 $\hbar\Omega_R$. The recorded PL spectra are plotted in Figs. 2c-e and depict the dispersion relations along the high symmetry directions K-Γ-K′, K′-M-K and K-K-K, respectively. The optical power density used for the pulsed excitation amounts to $\sim$ 10 Wcm^{-2}. Under consideration of nearest-neighbor and second-nearest neighbor coupling, the full dispersion relation of a particle in the S-band of a honeycomb lattice with lattice constant a reads in the TB treatment:

$$E_{hc}(\boldsymbol{k}_{||}) = E_0 \pm t\sqrt{3 + f(\boldsymbol{k}_{||})} - t' f(\boldsymbol{k}_{||}), \qquad (1)$$

$$f(\boldsymbol{k}_{||}) = 2\cos(\sqrt{3}k_y a) + 4\cos(\frac{\sqrt{3}}{2}k_y a)\cos(\frac{3}{2}k_x a). \qquad (2)$$

All dispersions are successfully described by the TB-fit using one single set of interaction parameters for the nearest-neighbor $t = 174$ μeV and second-nearest neighbor hopping $t' = -26$ μeV. These values are very similar to the ones found by Jacqmin *et al.* for a fully etched honeycomb lattice ($t = 250$ μeV, $t' = -20$ μeV) [25]. In particular, in Fig. 2e the lowest lying band of our dispersion

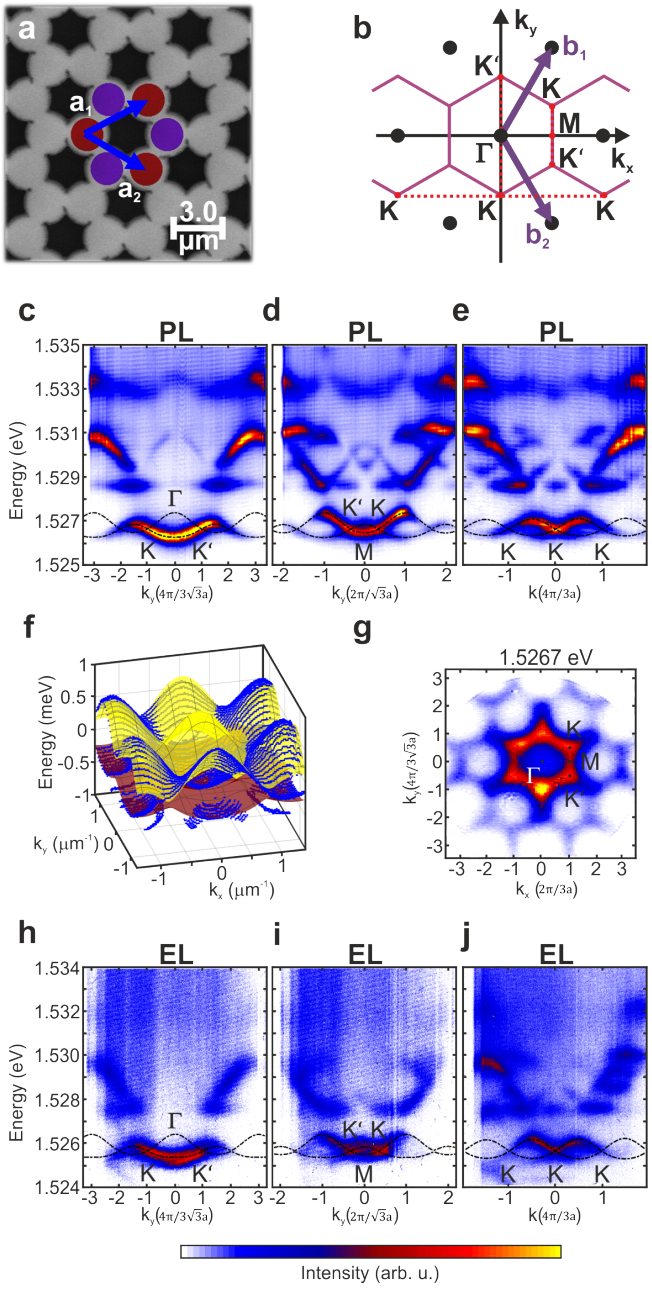

FIG. 2. (a) Scanning electron microscope image of the investigated honeycomb lattice and the corresponding reciprocal space (b). (c-e) PL dispersion in the K-Γ-K′ (c), K′-M-K (d) and K-K-K direction (e) of the 1st Brillouin zone (BZ), showing the distinct Dirac cone dispersion around the K-points. The dashed line is a tight-binding (TB) calculation reproducing the S-band of the dispersions. The excitation density amounts to $\sim$ 10 Wcm^{-2}. (f) Hyperspectral imaging of the 1st BZ with the peak positions fitted to the dispersion spectra (blue) and the TB simulation of the lower (red) and upper S-band (yellow). (g) Energy cut in reciprocal space at the center of the S-band, showing a clear honeycomb geometry with the K and K′ points. (h-j) EL emitted by the very same honeycomb lattice in the K-Γ-K′ (h), K′-M-K (i) and in the K-K-K (j) direction of the 1st BZ. The TB calculation uses the same fit parameter as for the PL measurement.

around the energetically degenerate K and K′ points at the corner of the 1st BZ features the characteristic Dirac cone dispersion of massless particles, stemming from the two-element basis of the lattice. In Fig. 2f, we show a hyperspectral image of the full (k_x, k_y)-dispersion highlighting the dispersion data points extracted from single measurements (blue) and the corresponding bonding π (red) and anti-bonding π^* (yellow) orbitals extracted from the TB model. The measured dispersion is in excellent agreement with the model. An energy cut in reciprocal space at the center of the S-band, showing a clear honeycomb geometry with the K and K′ points, is depicted in Fig. 2g. EL measurements of our polaritonic graphene are depicted in Figs. 2h-j, recorded along the K-Γ-K′, K′-M-K and K-K-K direction, respectively. Here, we apply a voltage yielding an averaged current density of 4.6 A/cm^2 flowing through our device. The injected current density in this experiment is well-compatible with strong coupling conditions in our device, as revealed in a control experiment on a standard 20 μm pillar (Supplementary Material, Fig. S3, which includes Refs. [36, 40, 41]). We observe an excellent agreement between the measurements using optical and electrical pumping, and the TB model. More importantly, our electrically injected polariton graphene features well-developed Dirac cones, as well as the flatband dispersion in the P-band.

In order to support the fact that arbitrary lattices can easily be realized, a similar analysis on a square lattice can be found in the Supplementary Material, which includes Refs. [36, 42–44].

B. Crossing the Threshold to Nonlinear Emission in the Honeycomb Lattice

A crucial step towards the applicability of our device platform for the use of polaritonic simulation, which facilitates the ultra-fast dynamics of the condensation process, as well as the implementation of topological polariton lasing, involves the demonstration of nonlinear threshold behavior in the input-output response [20, 21]. In order to optimally benefit from the narrowband resonance in our cavity device provided by the high photonic quality factor, we extended our study to a far-red-detuned honeycomb device (∼-30 meV). Upon increasing the injected current density, we observe a distinct redshift of the EL spectrum due to ohmic heating below threshold, which prevents the onset of lasing. This can be mitigated by providing a background gain via the incoherent non-resonant Ti:sapphire laser that homogenously illuminates the sample, as specified in the experiment section. The excitation density was chosen to ∼ 90 Wcm^{-2}, which is safely below the threshold density of ∼ 105 Wcm^{-2} at this detuning in the absence of electrical injection. These conditions put the lasing threshold within reach for electrical excitation and upon increasing the injected current density, we observe the onset of well pronounced, monochromatic emission features, which superimpose the luminescence spectrum of the lattice band structure, which is plotted along the M-Γ-M direction in Fig. 3a. We note that the spots of most intense luminescence correlate with the high-symmetry Γ points located in the 2nd BZ of the honeycomb lattice (see Fig 3b), which corresponds to the Bloch-mode within the higher Bloch band (P-band). Apparently, this Bloch-state provides optimal conditions for the maximal gain and results in its strong occupation. We note that polaritonic condensation into higher Bloch states was observed in a 1D chain of trapping potentials [45]. To analyze the current density dependent emission in more detail, we extracted spectra around $k_x = 4\pi/3a$, and plotted the spectrally integrated intensity as a function of the injected current density in Fig. 3c. The clear threshold characteristic reflects the photonic nonlinearity in our polaritonic graphene, which places our electrically driven device within the zoo of nonlinear photonic on-chip simulators.

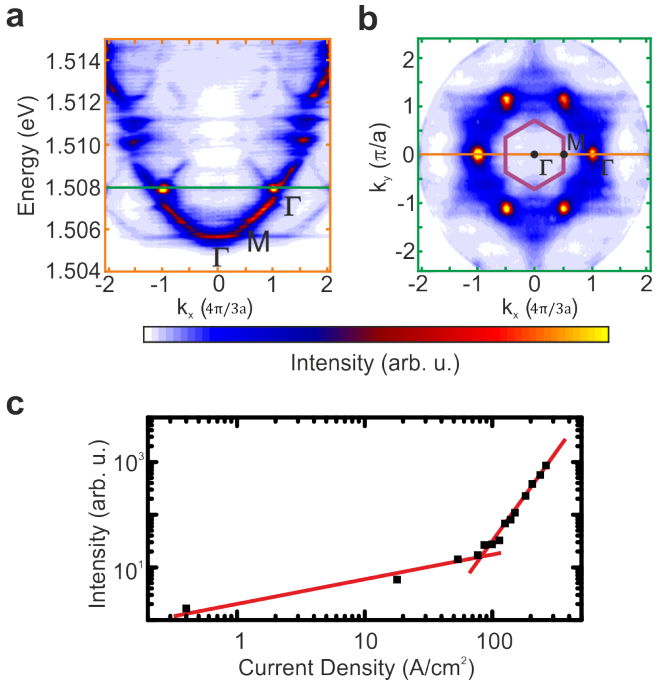

FIG. 3. (a) Luminescence dispersion of the honeycomb lattice in M-Γ-M direction under combined electrical and optical excitation. The constant laser power amounts to 90 Wcm^{-2}, while the injected current density amounts to 150 A/cm^2 here. With increasing current density a sharp emission in k-space as well as in energy is seen at the Γ-point of the 2nd Brillouin zone (BZ) at the bottom of the P-band. (b) Corresponding luminescence dispersion of the honeycomb lattice at a constant energy of 1.508 eV, as indicated by the green line in (a). The 1st BZ and the relevant high-symmetry points are highlighted. (c) Extracted intensity of the relevant mode under combined optical and electrical excitation. A nonlinear increase of the emission intensity is seen around a threshold density of ∼ 100 A/cm^2.

IV. CONCLUSION AND OUTLOOK

In conclusion we have presented the first implementation of an electrically injected, lithographically defined lattice for bosonic quasiparticles, both in the square as well as the honeycomb geometry. The lattice features $\sim$ 250 coupled lattice sites, yielding the prospect for homogeneous driving of extended, arbitrary polariton potential landscapes. The high quality of our fabrication process is reflected in the excellent agreement between photo- and electroluminescence experiments. All acquired data can be reproduced by TB models. We observe well-developed Dirac cones in our electrically driven polariton graphene, besides a flatband dispersion in the P-band. Our device implementation is capable to demonstrate nonlinear behavior under combined electrical and optical excitation, which is a crucial step towards the implementation of bosonic annealing for ultra-fast simulation of the classical XY-Hamiltonian [21]. We further anticipate that our polariton graphene platform serves well as a platform for the implementation of electrically injected quantum Hall simulators, and related electrically injected topological lasers in the polariton platform [10, 46], promising convenient extension to Floquet topological matter [47].

ACKNOWLEDGMENTS

We acknowledge support by the ImPACT Program, Japan Science and Technology Agency, the State of Bavaria and by the German Research Foundation (DFG) within project SCHN1376/2-1, SCHN1376/3-1 and KL3124/2-1. S.K. acknowledges the European Commission for the H2020 Marie Sklodowska-Curie Actions (MSCA) fellowship (Topopolis). R.T. is supported by the DFG through SFB 1170 (project B04) and by the European Research Council through ERC-StG-TOPOLECTRICS-Thomale-336012. S.H. acknowledges support within the EPSRC Hybrid Polaritonics Grant (EP/M025330/1).

[1] C. Weisbuch, M. Nishioka, A. Ishikawa,and Y. Arakawa, Phys. Rev. Lett. **69**, 3314-3317 (1992).
[2] A. Imamoglu, R. J. Ram, S. Pau, and Y. Yamamoto, Phys. Rev. A **53**, 4250 (1996).
[3] J. Kasprzak, M. Richard, S. Kundermann, A. Baas, P. Jeambrun, J. M. J. Keeling, F. M. Marchetti, M. H. Szymańska, R. André, J. L. Staehli, V. Savona, P. B. Littlewood, B. Deveaud, and Le Si Dang, Nature **443**, 409-414 (2006).
[4] R. Balili, V. Hartwell, D. Snoke, L. Pfeiffer, and K. West, Science **316**, 1007-1010 (2007).
[5] A. Amo, J. Lefrére, S. Pigeon, C. Adrados, C. Ciuti, I. Carusotto, R. Houdré, E. Giacobino, and A. Bramati, Nat. Phys. **5**, 805-810 (2009).
[6] Karzig, T., Bardyn, C.-E., Lindner, N. H. & Refael, G., Phys. Rev. X **5**, 031001 (2015).
[7] Bardyn, C.-E., Karzig, T., Refael, G. and Liew, T. C. H. Topological polaritons and excitons in garden-variety systems Phys. Rev. B **91**, 161413(R) (2015).
[8] Nalitov, A.V., Solnyshkov, D.D. & Malpuech, G. Polariton Z Topological Insulator. Phys. Rev. Lett. **114**, 116401 (2015).
[9] St-Jean, P., Goblot, V., Galopin, E., Lematre, A., Ozawa, T., Le Gratiet, L., Sagnes, I., Bloch, J. & Amo, A. Nat. Photonics **11**, 651656 (2017).
[10] Klembt, S., Harder, T. H., Egorov, O. A., Winkler, K., Ge, R., Bandres, M. A., Emmerling, M., Worschech, L., Liew, T. C. H., Segev, M., Schneider, C. & Höfling, S. Nature, DOI 10.1038/s41586-018-0601-5, (2018).
[11] H. Deng, G. Weihs, C. Santori, J. Bloch, and Y. Yamamoto, Science **298**, 199202 (2002).
[12] S. Christopoulos, G. Baldassarri Höger von Högersthal, A. J. D. Grundy, P. G. Lagoudakis, A. V. Kavokin, J. J. Baumberg, G. Christmann, R. Butté, E. Feltin, J.-F. Carlin, and N. Grandjean, Phys. Rev. Lett. **98**, 126405 (2007).
[13] Y.-Y. Lai, Y.-P. Lan, and T.-C. Lu, Appl. Phys. Express **5**, 082801 (2012).
[14] S. Kéna-Cohen, and S. R. Forrest, Nat. Photonics **4**, 371375 (2010).
[15] D. Bajoni, P. Senellart, A. Lemaître, and J. Bloch, Phys. Rev. B **76**, 201305 (2007).
[16] J. Gessler, V. Baumann, M. Emmerling, M. Amthor, K. Winkler, S. Höfling, C. Schneider, and M. Kamp, Appl. Phys. Lett. **105**, 181107 (2014).
[17] B. Zhang, S. Brodbeck, Z. Wang, M. Kamp, C. Schneider, S. Höfling, and H. Deng, Appl. Phys. Lett. **106**, 051104 (2015).
[18] C. P. Dietrich, A. Steude, M. Schubert, J. Ohmer, U. Fischer, S. Höfling, and M. C. Gather, Adv. Opt. Mater. **5**, 1600659 (2017).
[19] Y. Sun, P. Wen, Y. Yoon, G. Liu, M. Steger, L. N. Pfeiffer, K. West, D. W. Snoke, and K. A. Nelson, Phys. Rev. Lett. **118**, 016602 (2017).
[20] A. Amo, and J. Bloch, C. R. Phys. **17**, 934-945 (2016).
[21] N. G. Berloff, M. Silva, K. Kalinin, A. Askitopoulos, J. D. Töpfer, P. Cilibrizzi, W. Langbein, and P. G. Lagoudakis, Nat. Mat. **16**, 11201126 (2017).
[22] H. Ohadi, A. J. Ramsay, H. Sigurdsson, Y. del Valle-Inclan Redondo, S. I. Tsintzos, Z. Hatzopoulos, T. C. H. Liew, I. A. Shelykh, Y. G. Rubo, P. G. Savvidis, and J. J. Baumberg, Phys. Rev. Lett. **119**, 067401 (2017).
[23] T. Gao, E. Estrecho, K. Y. Bliokh, T. C. H. Liew, M. D. Fraser, S. Brodbeck, M. Kamp, C. Schneider, S. Höfling, Y. Yamamoto, F. Nori, Y. S. Kivshar, A. G. Truscott, R. G. Dall, and E. A. Ostrovskaya, Nature **526**, 554558 (2015).
[24] C. Schneider, K. Winkler, M. D. Fraser, M. Kamp, Y. Yamamoto, E. A. Ostrovskaya, and S. Höfling, Rep. Prog. Phys. **80**, 016503 (2017).
[25] T. Jacqmin, I. Carusotto, I. Sagnes, M. Abbarchi, D. D. Solnyshkov, G. Malpuech, E. Galopin, A. Lemaître, J.

Bloch, and A. Amo, Phys. Rev. Lett. **112**, 116402 (2014).
[26] M. Bayer, T. Gutbrod, A. Forchel, T. L. Reinecke, P. A. Knipp, R. Werner, and J. P. Reithmaier, Phys. Rev. Lett. **83**, 5374 (1999).
[27] G. Dasbach, M. Bayer, M. Schwab, and A. Forchel, Semicond. Sci. Technol. **18**, 339-350 (2003).
[28] N. Y. Kim, K. Kusudo, C. Wu, N. Masumoto, A. Löffler, S. Höfling, N. Kumada, L. Worschech, A. Forchel, and Y. Yamamoto, Nat. Phys. **7**, 681686 (2011).
[29] K. Winkler, J. Fischer, A. Schade, M. Amthor, R. Dall, J. Geler, M. Emmerling, E. A. Ostrovskaya, M. Kamp, and C. Schneider, New J. Phys. **17**, 023001 (2015).
[30] S. Klembt, T. H. Harder, O. A. Egorov, K. Winkler, H. Suchomel, J. Beierlein, M. Emmerling, C. Schneider, and S. Höfling, Appl. Phys. Lett. **111**, 231102 (2017).
[31] C. E. Whittaker, E. Cancellieri, P. M. Walker, D. R. Gulevich, H. Schomerus, D. Vaitiekus, B. Royall, D. M. Whittaker, E. Clarke, I. V. Iorsh, I. A. Shelykh, M. S. Skolnick, and D. N. Krizhanovskii, Phys. Rev. Lett. **120**, 097401 (2018).
[32] N. Masumoto, N. Y. Kim, T. Byrnes, K. Kusudo, A. Löffler, S. Höfling, A. Forchel, and Y. Yamamoto, New J. Phys. **14**, 065002-065009 (2012).
[33] K. Kusudo, N. Y. Kim, A. Löffler, S. Höfling, A. Forchel, and Y. Yamamoto, Phys. Rev. B **87**, 214503 (2013).
[34] A. H. Castro Neto, F. Guinea, N. M. R. Peres, K. S. Novoselov, and A. K. Geim, Rev. Mod. Phys. **81**, 109-162 (2009).
[35] S. I. Tsintzos, N. T. Pelekanos, G. Konstantinidis, Z. Hatzopoulos, and P. G. A. Savvidis, Nature **453**, 372375 (2008).
[36] C. Schneider, A. Rahimi-Iman, N. Y. Kim, J. Fischer, I. G. Savenko, M. Amthor, M. Lermer, A. Wolf, L. Worschech, V. D. Kulakovskii, I.A. Shelykh, M. Kamp, S. Reitzenstein, A. Forchel, Y. Yamamoto, and S. Höfling, Nature **497**, 348352 (2013).
[37] P. Bhattacharya, B. Xiao, A. Das, S. Bhowmick, and J. Heo, Phys. Rev. Lett. **110**, 206403 (2013).
[38] H. Suchomel, S. Brodbeck, T. C. H. Liew, M. Amthor, M. Klaas, S. Klembt, M. Kamp, S. Höfling, and C. Schneider, Sci. Rep. **7**, 5114 (2017).
[39] P. Tsotsis, S. I. Tsintzos, G. Christmann, P. G. Lagoudakis, O. Kyriienko, I. A. Shelykh, J. J. Baumberg, A. V. Kavokin, Z. Hatzopoulos, P. S. Eldridge, and P. G. Savvidis, Phys. Rev. Appl. **2**, 014002 (2014).
[40] S. Brodbeck, H. Suchomel, M. Amthor, A. Wolf, M. Kamp, C. Schneider, and S. Höfling, Appl. Phys. Lett. **107**, 041108 (2015).
[41] T. Gutbrod, M. Bayer, A. Forchel, J. P. Reithmaier, T. L. Reinecke, S. Rudin, and P. A. Knipp, Phys. Rev. B **57**, 9950-9956 (1998).
[42] K. Winkler, O. A. Egorov, I. G. Savenko, X. Ma, E. Estrecho, T. Gao, S. Müller, M. Kamp, T. C. H. Liew, E. A. Ostrovskaya, S. Höfling, and C. Schneider, Phys. Rev. B **93**, 121303(R) (2016).
[43] D. Tanese, H. Flayac, D. Solnyshkov, A. Amo, A. Lemaître, E. Galopin, R. Braive, P. Senellart, I. Sagnes, G. Malpuech, and J. Bloch, Nat. Comm. **4**, 1749 (2013).
[44] M. Sich, J. K. Chana, O. A. Egorov, H. Sigurdsson, I. A. Shelykh, D. V. Skryabin, P. M. Walker, E. Clarke, B. Royall, M. S. Skolnick, and D. N. Krizhanovskii, Phys. Rev. Lett. **120**, 167402 (2018).
[45] T. Gao, E. Estrecho, G. Li, O. A. Egorov, X. Ma, K. Winkler, M. Kamp, C. Schneider, S. Höfling, A. G. Truscott, and E. A. Ostrovskaya, Phys. Rev. Lett. **117**, 097403 (2016).
[46] T. Ozawa, H. M. Price, A. Amo, N. Goldman, M. Hafezi, L. Lu, M. Rechtsman, D. Schuster, J. Simon, O. Zilberberg, and I. Carusotto, arXiv:1802.04173 (2018).
[47] Rechtsman, M. C., Zeuner, J. M., Plotnik, Y., Lumer, Y., Podolsky, D., Dreisow, F., Nolte, S., Segev, M. & Szameit, A. Nature **496**, 196 (2013).